Prell, W.L., Wang, P., Blum, P., Rea, D.K., and Clemens, S.C. (Eds.)
Proceedings of the Ocean Drilling Program, Scientific Results Volume 184

12. Geochemistry of Pliocene Sediments from ODP Site 1143 (Southern South China Sea)[1]

Rolf Wehausen,[2] Jun Tian,[3] Hans-Jürgen Brumsack,[2] Xinrong Cheng,[3] and Pinxian Wang[3]

ABSTRACT

Pliocene core intervals from Ocean Drilling Program Site 1143 located in the southern part of the South China Sea were measured for their major and minor element composition at ~2-k.y. resolution. Changes in sediment composition parallel glacial–interglacial changes as indicated by the corresponding oxygen isotope record of benthic foraminifers. Carbonate contents are lower during glacial stages and higher during interglacial stages. This is attributed to dilution by a higher contribution of terrigenous detrital matter during glacial intervals and to enhanced biological productivity during interglacials as indicated by enrichments in barium. The terrigenous detrital matter fraction shows small but distinct changes in composition. These variations may be explained by multiple processes, including changes in provenance and weathering caused by monsoonal climate variability and sea level fluctuations. Gradual or long-term changes in sediment composition also occur during the investigated interval. There is a shift toward lower TiO_2 (carbonate-free basis; cfb) values at around 2.9 Ma and an increase in Al_2O_3 (cfb) variations at around 2.55 Ma. These changes can be explained in both cases by an increasing contribution from the Mekong River, delivering material with low TiO_2 (cfb)/Al_2O_3 (cfb) ratios, followed by a gradual increase in weathering, causing higher Al_2O_3 (cfb) (probably reflecting kaolinite) contents. Both may be the result of an enhanced summer monsoon. The manganese and phosphate geochemistry of Site 1143 sediments seem to be strongly dominated by biological productivity and a high burial flux of carbonate,

[1]Wehausen, R., Tian, J., Brumsack, H.-J., Cheng, X., and Wang, P., 2003. Geochemistry of Pliocene sediments from ODP Site 1143 (southern South China Sea). *In* Prell, W.L., Wang, P., Blum, P., Rea, D.K., and Clemens, S.C. (Eds.), *Proc. ODP, Sci. Results*, 184, 1–25 [Online]. Available from World Wide Web: <http://www-odp.tamu.edu/publications/184_SR/VOLUME/CHAPTERS/201.PDF>. [Cited YYYY-MM-DD]
[2]Institut für Chemie und Biologie des Meeres (ICBM), Carl-von-Ossietzky-Universität, D-26111 Oldenburg, Germany. Correspondence author: **wehausen@icbm.de**
[3] Key Laboratory of Marine Geology, MOE, Tongji University, Shanghai, 200092 People's Republic of China.

Initial receipt: 8 August 2001
Acceptance: 26 June 2002
Web publication: 6 February 2003
Ms 184SR-201

which acts as an adsorbing agent and/or substrate. During strong interglacials and corresponding times of enhanced productivity, Mn may be remobilized from continental margin sediments deposited within an oxygen minimum zone and subsequently exported into the pelagic region, where it oxidizes and settles to form Mn-enriched layers in the sediment.

INTRODUCTION

During Ocean Drilling Program (ODP) Leg 184, six sites were drilled in two areas of the South China Sea. The major aim of ODP Leg 184 was to reconstruct the evolution and variability of the East Asian monsoon to better understand the links between tectonic uplift, monsoons, and global climate variation (Wang, Prell, Blum, et al., 2000). Site 1143 is located in the southern part of the basin. It was chosen to capture the long-term record of sediment accumulation rates and lithologic variability associated with the Mekong and Sunda River systems, which might be related to the uplift and denudation of Tibetan and East Asian tectonic systems (Wang, Prell, Blum, et al., 2000).

Except for surface sediment studies (Calvert et al., 1993), inorganic geochemical studies of South China Sea sediments are rare. In this chapter, we present major and minor element data of Pliocene cores from ODP Site 1143. These data provide information on the relative contribution of terrigenous detrital matter from different provenances (e.g., Wehausen and Brumsack, 1999) or of weathering intensity (e.g., Schneider et al., 1997). Furthermore, variations in biological productivity or diagenesis can be reconstructed based on barium (Dehairs et al., 1980; Dymond et al., 1992), phosphorus (Delaney, 1998), or redox-sensitive trace element abundance (Calvert and Pedersen, 1993). The oxygen isotope stratigraphy of **Tian et al.** (this volume) provides a stratigraphic framework that will be applied to interpret changes in sediment geochemistry with respect to glacial–interglacial stages. A comparison of elemental proxy data with the benthic oxygen isotope curve may provide information about the relationship between terrigenous input, monsoons, sea level changes, and glacial climates.

MATERIALS AND METHODS

Sample Description

For the present study, late Pliocene sediment cores from ODP Site 1143 were sampled at 10-cm resolution. At a sedimentation rate of ~4.5 cm/k.y. (Shipboard Scientific Party, 2000), this equals a temporal resolution of ~2 k.y. Site 1143 is located in a water depth of 2772 m in the Nansha Islands or Dangerous Grounds area (Fig. **F1**). This area is riddled with reefs, shoals, and small islands. Some of the islands are within 20 to 30 mi of the site (Shipboard Scientific Party, 2000). Site 1143 is also located within the region of relatively stable and warm sea-surface temperatures, the West Pacific Warm Pool. The most important sediment source for the southern South China Sea is the Mekong River (Fig. **F1**), with a draining area of 810,000 km², delivering 160 million tons of sediment per year (Milliman and Meade, 1983). Smaller rivers of Borneo may also contribute material to the Site 1143 area. During sea level lowstand, rivers from the emerging shelf have also contributed material to

F1. Map showing sites in South China Sea, p. 15.

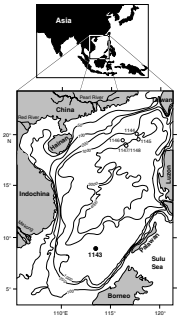

the sediments of the southern South China Sea (Molengraaff, 1921). Assuming a mineral aerosol flux equal to or less than the estimated modern value (0.5 g/cm² per k.y.) (Duce et al., 1991), eolian sediment contributions, at maximum, may account for 12% of the total sediment accumulation (~4.1 g/cm² per k.y.) (Shipboard Scientific Party, 2000).

A primary productivity of 300 to 500 g C/m² per day has been observed for periods of upwelling (spring/summer) in the Nansha Islands area. The annual average is 100 to 200 g C/m² per day (Guo, 1994).

Analytical Procedures

Prior to chemical analysis, the samples were freeze-dried, ground, and homogenized in agate ball mills. For X-ray fluorescence (XRF) analysis, 600 mg of the sample powder was mixed with 3600 mg dilithium tetraborate ($Li_2B_4O_7$, Spectromelt by Merck), preoxidized at 500°C with NH_4NO_3, and fused to glass beads in Pt crucibles. For the analysis of sulfur in three selected samples, a mixture of 50% lithium tetraborate and 50% lithium metaborate (Spectroflux by Alpha) was used as a flux. All the beads were analyzed using a Philips PW 2400 X-ray spectrometer. Calibration was done with a set of up to 50 carefully chosen international reference samples. Analytical precision, as checked by parallel analysis of one international (GSR-6) and several in-house standards, was <1% for major and <4% for minor elements (except for As and Co; 10%).

Total carbon (C_{total}) contents of selected samples were determined by coulometric titration following combustion with a Stöhlein-Instrument. Analytical precision of this method was <3%. Carbonate carbon (C_{carb}) was determined by coulometric titration following release of CO_2 with 2-N $HClO_4$ at 70°C with a UI-carbon analyzer. The analytical precision of this method was <3%. Total organic carbon values were calculated as the difference between C_{total} and C_{carb} (Prakash Babu et al., 1999).

Calculations and Stratigraphy

Calcium carbonate contents were estimated for all samples based on the assumption that all Ca is present as calcite ($CaCO_3 = CaO \times 1.7848$). This approach is supported by the good correlation between CaO contents obtained by XRF and C_{carb} values obtained by coulometry (Fig. F2).

F2. Correlation of CaO and C_{carb} values, p. 16.

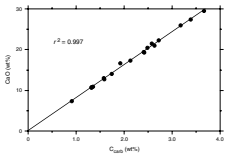

Elemental contents were calculated on a carbonate-free basis for each sample according to the following equation:

$$[\text{Element (oxide)}]\ \text{cfb} = [\text{Element (oxide)}]\ \text{tot}/100 - CaCO_3,$$

where

[Element (oxide)] cfb = content of an element or element oxide in the sample calculated on a carbonate-free basis,
[Element (oxide)] tot = total content of an element or element oxide in the sample, and
$CaCO_3$ = content of $CaCO_3$ calculated as described above.

For geochemical comparison and as an age model, we use the oxygen isotope record of **Cheng et al.** (this volume) and the stratigraphy of **Tian et al.** (this volume). The data set is based on measurements of the

benthic foraminifer species *Cibicidoides wuellerstorfi* (one to three specimens of 0.3 to 0.9 mm in diameter) in a core sampling interval of 10 cm (**Cheng et al.,** this volume). The chronological framework is based on the comparison of the benthic $\delta^{18}O$ record with the 6-Ma composite oxygen isotope curve provided by Shackleton (**Tian et al.,** this volume). Essentially, the part of the stratigraphy between 1.811 and 6 Ma is based on the comparison with ODP Site 846 data (Shackleton et al., 1995a, 1995b).

RESULTS AND DISCUSSION

All inorganic geochemical data discussed in this publication are listed in Table **T1**. The most important aspects of the data set are presented and discussed below.

T1. Inorganic geochemical data, p. 25.

Sediment Bulk Composition

The investigated sediments may be regarded as clay or calcareous nannofossil-rich clay with carbonate contents between 5 and 30 wt%. According to our own data (Table **T1**) as well as shipboard measurements (Shipboard Scientific Party, 2000), the organic carbon contents vary between 0.2 and 0.5 wt%, suggesting permanently oxygenated conditions at the seafloor and a moderate organic carbon flux.

In a ternary plot (Fig. **F3**), which shows the relative proportions of SiO_2 (representing quartz or opaline silica), Al_2O_3 (representing clay minerals), and CaO (representing carbonate), the sediments can be described as mixtures of biogenous carbonate with an aluminosilicate component that has a slightly higher Al content than average shale. Sediments and soils consisting of highly weathered material—predominantly found in tropical regions—are known for their high Al contents (Mason and Moore, 1985). Because there are no samples plotting toward higher SiO_2 contents in the ternary plot, quartz and biogenic silica fractions are rather low or negligible (Fig. **F3**).

F3. SiO_2, Al_2O_3, and CaO contents, p. 17.

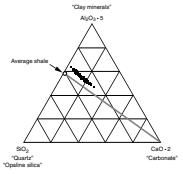

In contrast to sediments from ODP Site 1145, which show a certain eolian (loess) influence (Wehausen and Brumsack, 2002), sediments from Site 1143 presented here are characterized by relatively low TiO_2/Al_2O_3 ratios (Fig. **F4**). Whereas Site 1145 samples plot closer to the dilution line for loess (Schnetger, 1992), Site 1143 samples plot toward higher Al_2O_3 values, relatively close to the data point for Mekong suspended matter (SPM) (Martin and Meybeck, 1979). However, in addition to material from the Mekong River, there seems to have been at least one other source with slightly higher Ti and lower Al contents delivering material to this part of the South China Sea because all samples plot above the ratio for Mekong SPM (Fig. **F4**).

F4. Correlation of TiO_2 and Al_2O_3, p. 18.

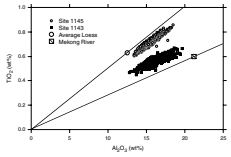

Changes in Sediment Composition vs. Time

Depth profiles of $CaCO_3$, SiO_2, and Al_2O_3 contents demonstrate that the bulk composition of the sediments show a high variability with time (Fig. **F5**). SiO_2 and Al_2O_3 display the same pattern (correlation coefficient: $r^2 = 0.92$), which again shows that there is no significant contribution of biogenic opal to the total SiO_2 content. Only very few diatoms and radiolarians were found in the late Pliocene sediments of Site 1143 (Shipboard Scientific Party, 2000).

F5. $\delta^{18}O$ and bulk geochemical data, p. 19.

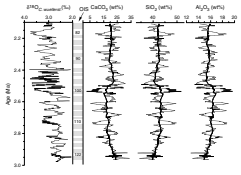

With regard to the carbonate contents, two different types of carbonate cycles have been reported for South China Sea sediments (Thunell et al., 1992). Carbonate cycles with higher carbonate contents during glacials ("Pacific type"), reflecting the varying carbonate compensation depth (CCD) or lysocline, are only observed in sediments deposited in water depths below 3500 m. Classical carbonate cycles, showing lower carbonate content during glacials due to dilution by terrigenous detrital material and higher carbonate contents during interglacials ("Atlantic type") (Thunell et al., 1992), are found in water depths above 3000 m. At present, the water depth of Site 1143 is 2772 m. Assuming a similar depth during the Pliocene (permanent sedimentation above the CCD), "Atlantic-type" carbonate cyclicity should be expected at this location. Our data show that carbonate contents are generally lower and terrigenous detrital matter (SiO_2 and Al_2O_3) contents are higher during glacial stages (Fig. F5). This supports "Atlantic-type" carbonate cycles mode (i.e., dilution cycles). Minimum carbonate and maximum terrigenous detrital matter contents are observed for oxygen isotope Stages 100, 104, 106, and 110. Beyond some small peaks in sediment composition (i.e., changes of short duration), the carbonate terrigenous detrital matter relationship displays low variability before 2.85 Ma (Fig. F5).

Changes in Terrigenous Detrital Matter Composition

In order to define changes in the composition of the terrigenous detrital matter, we either use elemental contents that were calculated on a carbonate-free basis (see "Materials and Methods," p. 2) or ratios of terrigenous detrital elements.

In general, slight changes in the composition of terrigenous detrital matter are discernible. A few distinct thin layers show significantly lower contents of most major components of the noncarbonate fraction (Fig. F6). TiO_2 (cfb) displays a relatively strong variation throughout the investigated interval. A shift toward lower TiO_2 (cfb) values occurs at ~2.9 Ma. SiO_2 (cfb) and K_2O (cfb) covary more or less with TiO_2 (cfb) but show relatively little variability. The Al_2O_3 (cfb) content displays only small variations in sediments older than 2.6 Ma. In the upper part of the core, variations are stronger with an opposite pattern compared to SiO_2 (cfb), TiO_2 (cfb), and K_2O (cfb) (Fig. F6A).

The Si/Al ratio shows low variations in sediments >2.6 Ma and higher variation in sediments <2.6 Ma (Fig. F6A). In contrast, Ti/Al displays strong variations throughout the whole section (Fig. F6B), mainly driven by the TiO_2 (cfb) content with relatively high amplitude variations (Fig. F6A). K/Al, Cr/Al, Rb/Al, and Zr/Al ratios covary more or less with the Ti/Al ratio, and all five parameters display long-term changes. They decrease between 2.9 and 2.5 Ma and slightly increase again thereafter.

To observe and interpret those changes in terrigenous detrital matter composition with respect to global ice volume and sea level changes, we compared the Al_2O_3 (cfb) and TiO_2 (cfb) records with the benthic $\delta^{18}O$ curve (Fig. F7). Higher contents of Al_2O_3 (cfb) are present during glacial stages owing to an enhanced contribution of strongly weathered material from the Asian continent or adjacent islands. TiO_2 (cfb) contents, which are lower during glacials, are due to stronger fluvial input of material with low Ti content (e.g., suspended matter from Mekong River) (Martin and Meybeck, 1979). Until 2.8 Ma, a significant increase in Al_2O_3 (cfb) content is not seen. A weak enrichment in Al is visible at oxygen isotope Stage 110 (2.73 Ma), which marks the onset of major

F6. Terrigenous detrital elements and elemental ratios, p. 20.

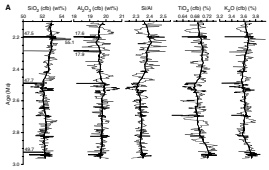

F7. $\delta^{18}O$ and terrigenous detrital elements, p. 22.

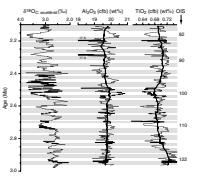

glaciation cycles of the Northern Hemisphere (Tiedemann et al., 1994). Amplitudes of Al_2O_3 (cfb) content increase after 2.55 Ma, and the strongest Al enrichments are present during isotope Stages 100, 96, and 82. The highest amplitudes and, thus, the strongest minima are present in the TiO_2 (cfb) record between 2.45 and 2.8 Ma.

What are the climatic and/or oceanographic mechanisms causing changes in terrigenous detrital matter composition? There are four possible scenarios, as known from earlier publications and described in the following paragraphs.

1. Changing weathering conditions on the continent. Sediments from the Zaire Fan display cyclic changes in the Al/K ratio, which Schneider et al. (1997) interpreted as fluctuations in weathering intensity related to variations in the West African monsoon. The Al/K ratio served as an indicator for the dominance of kaolinite, an important product of intensive weathering, over feldspar (or other K-bearing minerals). By applying this geochemical indicator, it was demonstrated that increased central African heating during astronomical insolation maxima led to a stronger monsoonal precipitation (Schneider et al., 1997).

   The chemical index of alteration (CIA) (Nesbitt and Young, 1982) in sediments from the Bay of Bengal was found to be related to chemical weathering driven by the Asian summer monsoon (Colin et al., 1998). The CIA is calculated from Al, Ca, Na, and K contents.

   These two examples show that monsoon-related weathering intensity can affect the relative abundances of major elements in the terrigenous detrital fraction of sediments. For the South China Sea, weathering may also explain changes in the Al_2O_3 (cfb) contents as seen in Figure F7 but will probably fail to explain, for example, SiO_2 (cfb) and TiO_2 (cfb) profiles. These show distinct patterns that can not be explained by variations in weathering-related clay mineral composition (i.e., Al, Na, or K contribution) alone. If weathering would be the only mechanism causing differences in the composition of the terrigenous detrital matter composition, then SiO_2 (cfb) and TiO_2 (cfb) profiles would probably display an exactly reverse pattern compared to the Al_2O_3 (cfb) profile because of the closed sum effect within the terrigenous detrital matter fraction. Owing to their occurrence in more weathering-resistant minerals (e.g., quartz, rutile, and ilmenite), Si and Ti contents are not dominated by weathering effects. Therefore, these two elements should not display a distinct pattern, as is the case for the sediments investigated here. As a consequence, changes in weathering intensity may only form one part of the answer.

2. Variations in provenance (e.g., stronger riverine contribution during maxima in summer monsoon). Several studies demonstrated that differences in provenance are seen in the major element geochemistry of sediments. For example, Shimmield and Mowbray (1991) were able to identify monsoon-related changes in the eolian flux into Arabian Sea sediments through elemental ratios like Ti/Al and Cr/Al. Similarly, Wehausen and Brumsack (1999) used Mg/Al, K/Al, and other element ratios to show that the relative contribution of eolian and fluvial sources to the east-

ern Mediterranean varied due to more arid or humid climate conditions on the African and southern European continents. For the Site 1143 data discussed here, fluctuations in the TiO_2 (cfb) content, K_2O (cfb) content, Cr/Al ratio, and Rb/Al ratio may also be explained by two different sources (e.g., either the Mekong River or rivers from Borneo delivering more or less material depending on monsoonal variations). However, if there were in fact two (or more) different sources, they should be characterized by material that is very similar in composition because the detected variability in sediment composition is only of minor importance.

In contrast to Arabian Sea (Shimmield and Mowbray, 1991) or eastern Mediterranean (Wehausen and Brumsack, 1999) sediments, Site 1143 sediments are strongly dominated by fluvial input, because the eolian contribution is low for this part of the South China Sea (see **"Sample Description,"** p. 2, in "Materials and Methods"). Compared to eolian fluxes (Rea, 1994), fluvial contributions to distal sites like Site 1143 depend much more on water currents as well as basin and river fan structures, both of which are influenced by sea level. Therefore, source strength cannot be assessed adequately without discussing the following two points.

3. Changes in the strength and direction of water currents. The influence of surface-water circulation on sediment dispersal has been discussed in earlier publications. One example seems to be reflected in sediments from the Ceara Rise, in the equatorial western Atlantic (Tiedemann and Franz, 1997). Here, the current system off Brazil, which is mainly influenced by the latitudinal position of the intertropical convergence zone, has a strong influence on the transport of suspended sediment from the Amazon River to the Ceara Rise. In the modern eastern Mediterranean, the complicated current and water circulation system, for example, is responsible for a distinct dispersal pattern of terrigenous matter from several fluvial sources (Venkatarathnam and Ryan, 1971). In the past, changes in current directions seem to have led to significant changes in sediment distribution patterns (Wehausen and Brumsack, 2000).

   To our knowledge, data on dispersal tracks of the major riverine sediment sources of the South China Sea as related to current directions are not available. However, the surface-water circulation of the South China Sea is mainly driven by the annually reversing monsoon winds (Huang et al., 1994). During the summer monsoon, a rather clockwise surface circulation, which also reaches the bottom area of the shelf (Huang et al., 1994), may deflect the strengthened monsoonal runoff from the Mekong River toward the north. During winter monsoon, when Mekong River runoff is at its minimum, a counterclockwise circulation may deliver suspended matter from the shelf area of the southwestern part of the South China Sea to Site 1143. However, it remains questionable which of the two scenarios could have led to a higher contribution of suspended matter to Site 1143. Furthermore, the system becomes more complicated when eustatic sea level fluctuations are taken into account.

Strong bottom currents may have an additional influence on sediment composition via winnowing or focusing. Such phenomena led to the loss or accumulation of the fine fraction at the sediment surface. Usually, such deposits are characterized by layers significantly enriched or depleted in heavy mineral-related elements like Zr. Contents of this element strongly depend on grain size sorting effects (Wehausen, 1999). Although turbidites are a common feature, especially in the older sediments of Site 1143 (Shipboard Scientific Party, 2000), no such layers were detected in the core sections investigated in the present work.

4. Sea level changes. Because of the presence of a large shelf area in its southern part, the South China Sea became a semienclosed basin during the last glacial maximum with significant consequences regarding water circulation patterns (Wang and Wang, 1990). At that time the drastic sea level lowering also led to erosion of material from the exposed shelf. This material was transported via the Paleo-North Sunda River system (Wang et al., 1995) more or less directly into the present deep central basin. As another consequence, material from the exposed Sunda shelf, with a different composition compared to material from Mekong River, presumably has influenced terrigenous detrital matter composition at Site 1143. Additionally, the Mekong River delta shifted eastward, probably also leading to a higher suspended matter contribution to Site 1143. The overall consequence must have been an increase in terrigenous detrital matter accumulation in the area around Site 1143.

   Although sea level changes as related to global ice volume were much weaker during the late Pliocene (Tiedemann et al., 1994), certain fluctuations in the size of the shelf area and the position of the Mekong River delta must have occurred. During glacial stages, a slightly enhanced sediment discharge is seen. This explains the higher contents of terrigenous detrital matter and lower contents of carbonate (Fig. F5). Perhaps it may also explain the higher Al_2O_3 (cfb) contents because Mekong riverine suspended matter is relatively enriched in Al when compared to crustal or average shale abundances (Taylor and McLennan, 1985; Wedepohl, 1971).

   However, this scenario alone does not account for differences in detrital element profile patterns and global ice volume. At least a combined influence of two different mechanisms, either climate related (changes in weathering intensity or varying sources) or oceanography-related (changes in sea level, basin structure, or water currents), must have operated simultaneously.

Biomediated Elements

The Ba content calculated on a carbonate-free basis or the Ba/Al ratio are parameters that may serve as indicators for paleoproductivity (Dymond et al., 1992; Francois et al., 1995). Both show exactly the same cyclic profile, but we prefer to use Ba/Al ratios for the sake of a better comparability with other studies where this proxy has been applied (Wehausen and Brumsack, 1999; Shimmield and Mowbray, 1991). Before using such Al-normalized total Ba contents as a proxy for marine

productivity conditions, it has to be evaluated whether the fluctuations are solely related to changes in terrigenous input, are only caused by variations in barite preservation (Schenau et al., 2001), or are indicative of real changes in barium flux rates and oceanic productivity. From other marine geochemical studies (Wehausen and Brumsack, 1999; Shimmield and Mowbray, 1991), as well as from the composition of the Earth's upper crust (Taylor and MacLennan, 1985) or average shale (Wedepohl, 1971, 1991), we know that the background Ba/Al value, at maximum, should be 70×10^{-4}. Because of the relatively high Al contents typical of a region with intense tropical weathering (see **"Changes in Terrigenous Detrital Matter Composition,"** p. 5), the background value for the South China Sea is lower than it is for average shale or sediments from higher latitudes. The Ba/Al variability of the investigated sediments is higher than any reasonable lithogenic background value. Therefore, the peaklike Ba enrichments in the data set (Fig. **F8**) are likely caused by an enhanced bio-barite flux (Dehairs et al., 1980; Bishop, 1988; Gingele and Dahmke, 1994) and thus could be used as a proxy for paleoproductivity. Certainly, the preservation of barite as determined by the degree of saturation in bottom and pore waters is an important factor influencing the Ba contents of marine sediments (McManus et al., 1998; Schenau et al., 2001). However, when pore water sulfate concentrations are more or less constant (i.e., under permanently oxic conditions), the degree of saturation itself is only controlled by the flux of barite (which acts as a positive feedback). Therefore, we do not believe that productivity and the associated barium flux were only constant or even lower when Ba enrichments are present in the sediment. Instead, a positive relationship between productivity and barium content of the sediments is most likely.

The Ba/Al ratio corresponds very well to the $\delta^{18}O$ curve. This indicates that productivity was lower during glacial stages and higher during interglacials. Exceptions are seen in the lower part of the core (during stages 110 and 120, productivity was slightly higher). The covariation between the Ba/Al ratio and carbonate content suggests that increases in carbonate contents during interglacial stages are not only due to less dilution but are also caused by enhanced biological production. Shimmield and Mowbray (1991) found a very good correlation between $\delta^{18}O$ of planktonic foraminifers, Ba/Al, and carbonate records for late Quaternary sediments from the northwest Arabian Sea. They proposed that the nutrient supply through upwelling of intermediate waters was the triggering factor for higher productivity during interglacials. A similar explanation may be valid for Site 1143 sediments, although we cannot solve the paleoclimatic and paleoceanographic mechanism causing a higher nutrient supply during interglacials in the southern South China Sea. One possibility may be the stronger inflow of nutrient-rich waters from the Sunda shelf. Another possibility is enhanced upwelling caused by stronger monsoonal winds.

The P/Al ratio displays a cyclic record that correlates with Ba/Al and carbonate contents (Fig. **F8**). The primary flux of phosphorus into marine sediments mainly appears in three different forms: organic material, fish remnants, and iron oxides that have a high adsorption capacity for phosphorus (Froehlich et al., 1988; Van Cappellen and Berner, 1988; Van Cappellen and Ingall, 1994). Lithogenic phosphorus is generally of minor importance. In deeper buried sediment layers phosphorus may still be present in these forms, but here, diagenetically formed carbonate-fluoroapatite (CFA) is responsible for the major fraction of phosphorus (Ruttenberg and Berner, 1993). About 80% of the

F8. Benthic foraminifer $\delta^{18}O$ record and records of biologically influenced element parameters, p. 23.

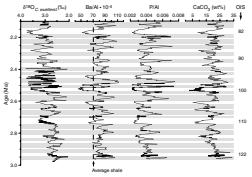

total P in Pliocene sediments from various settings were found to be present as CFA (Delaney, 1998).

Despite the dominance of authigenic phosphorus phases in deeper buried sediments, the covariation of P/Al ratio, carbonate content, and Ba/Al ratio suggests that the primary availability (i.e., changes in bioproductivity and phosphorus flux) had a significant influence on the phosphorus content of Site 1143 sediments. Another important factor for phosphorus burial is the carbonate content because the high surface area and adsorption capacity of calcite might trigger the formation of iron oxyhydroxide coatings, adsorbing agents for phosphorus (Delaney, 1998).

Redox-Sensitive and Chalcophile Elements

In general, Fe_2O_3 (cfb) contents display variations that covary with those of SiO_2 (cfb) (Figs. F9A, F6A). Besides these minor fluctuations caused by changes in terrigenous detrital matter composition, there are some small spikes and three very prominent peaks. These layers are characterized by lower terrigenous detrital matter contents (Fig. F6A) and enrichments in iron, sulfur, and the trace elements As, Co, and Ni (Fig. F9B). These trace elements are known to form stable sulfides or to coprecipitate with iron sulfides under sulfidic conditions (Jacobs and Emerson, 1985; Huerta-Diaz and Morse, 1992; Calvert and Pedersen, 1993). Vanadium, mainly present in the form of vanadyl cations in organic complexes under reducing conditions (Szalay and Szilagyi, 1967; Emerson and Huested, 1991), does not show a significant enrichment. All of this suggests the presence of pyrite and other metal sulfides of diagenetic origin in the form of small concretions that seem to have formed very locally. Evidence for microbial sulfate reduction was given by the pore water data (Shipboard Scientific Party, 2000).

High Mn/Al ratios well above the ratio for average shale and a partial covariation between Mn and carbonate contents (Fig. F9A) suggests the presence of manganese coatings on carbonate tests (Boyle, 1983; Franklin and Morse, 1983) or the presence of authigenic manganese carbonates (Thomson et al., 1986). Whereas Sr clearly correlates with $CaCO_3$ (r^2 = 0.96), Mn/Al displays a more specific behavior, probably caused by changes in terrigenous detrital matter flux. Furthermore, some enrichments in manganese are seen that cannot be explained by carbonate contents or terrigenous input. The Mn/Al peaks at 2180, 2210, 2260, and 2430 ka may, for example, represent periods of a strong import of Mn from the shelf. Such an Mn accumulation mechanism has been reported for the Cretaceous Indian Ocean (Thurow et al., 1992). Oxygen-deficient conditions led to the mobilization of Mn(II) from shelf sediments and transport via the oxygen minimum zone into deeper regions of the basin. Since the Mn enrichments occurred during interglacials and corresponding times of high bioproductivity, the existence of an enhanced oxygen minimum zone is very likely.

F9. Elements that may be overprinted by diagenesis or redox reactions, p. 24.

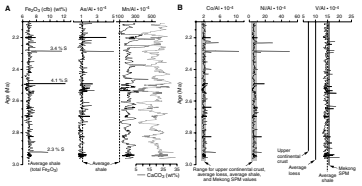

SUMMARY AND CONCLUDING REMARKS

Carbonate contents of late Pliocene sediments from Site 1143 display a cyclicity, with lower contents during glacial and higher contents during interglacial stages. Whereas dilution by terrigenous detrital matter input seems to be an important factor for low carbonate contents during glacials, enhanced productivity, indicated by Ba enrichments, seems

to have led to a higher carbonate flux during interglacials. The changes in productivity are probably associated with oceanographic changes (e.g., stronger inflow of nutrient-rich water masses from the Sunda shelf during interglacials).

The terrigenous detrital matter composition of Site 1143 sediments fluctuates owing to multiple processes, including changes in provenance and weathering intensity caused by monsoonal climate variability and sea level fluctuations, resulting in a varying shelf area and the Mekong River Fan structure.

A clear effect of the onset of major Northern Hemisphere glaciation cycles at 2.73 Ma (Tiedemann et al., 1994) on sediments from Site 1143 can not be observed, although gradual or long-term changes in sediment composition are present during the investigated interval. For example, there is a shift toward lower TiO_2 (cfb) values at ~2.9 Ma and an increase in Al_2O_3 (cfb) variations at ~2.55 Ma. These changes may be explained by an increasing contribution from the Mekong River, delivering material with low Ti/Al contents and a subsequent gradual increase in weathering, causing higher Al_2O_3 (cfb) (probably reflecting kaolinite) contents. Both could be the result of an enhanced summer monsoon.

The manganese and phosphate geochemistry of Site 1143 sediments seems to be strongly dominated by biological productivity and the availability of carbonate as an adsorbing agent for phosphate-rich iron oxides and/or substrates for the formation of manganese carbonates or CFA. During strong interglacials and corresponding times of enhanced productivity, Mn may be remobilized from continental margin sediments deposited within an oxygen-minimum zone and subsequently exported into the pelagic region, where it is oxidized and settles to form Mn-enriched layers in the sediment.

Pyrite concretions were detected as enrichments of iron, sulfide, and chalcophilic trace elements in the sediments. These layers are believed to be of minor significance and represent a rather small and locally restricted phenomenon.

ACKNOWLEDGMENTS

We would like to thank Berhard Schnetger (Institut für Chemie und Biologie des Meeres, Oldenburg) for analytical advice and the Scientific Party of ODP Leg 184 for their generous support and many stimulating discussions. Tracy D. Frank and an anonymous reviewer are thanked for helpful comments and suggestions. This research used samples and/or data provided by the Ocean Drilling Program (ODP). ODP is sponsored by the U.S. National Science Foundation (NSF) and participating countries under management of Joint Oceanographic Institutions (JOI), Inc. Funding for this research was provided by the Deutsche Forschungsgemeinschaft (DFG) (grant no. BR 775/11).

REFERENCES

Bishop, J.K.B., 1988. The barite-opal organic carbon association in oceanic particulate matter. *Nature,* 332:341–343.

Boyle, E.A., 1983. Manganese carbonate overgrowths on foraminifera tests. *Geochim. Cosmochim. Acta.,* 47:1815–1819.

Calvert, S.E., and Pedersen, T.F., 1993. Geochemistry of Recent oxic and anoxic marine sediments: implications for the geological record. *Mar. Geol.,* 113:67–88.

Calvert, S.E., Pedersen, T.F., and Thunell, R.C., 1993. Geochemistry of the surface sediments of the Sulu and South China Seas. *Mar. Geol.,* 114:207–231.

Colin, C., Kessel, C., Blamart, D., and Turpin, L., 1998. Magnetic properties of sediments in the Bay of Bengal and the Andaman Sea: impact of rapid North Atlantic Ocean climatic events on the strength of the Indian monsoon. *Earth Planet. Sci. Lett.,* 160:623–635.

Dehairs, F., Chesselet, R., and Jedwab, J., 1980. Discrete suspended particles of barite and the barium cycle in the open ocean. *Earth Planet. Sci. Lett.,* 49:528–550.

Delaney, M.L., 1998. Phosphorus accumulation in marine sediments and the oceanic phosphorus cycle. *Global Biogeochem. Cycles,* 12:563–572.

Duce, R.A., Liss, P.S., Merrill, J.T., Atlas, L.L., Buat-Menard, P., Hicks, B.B., Miller, J.M., Prospero, J.M., Arimoto, R., Church, T.M., Ellis, W., Galloway, J.N., Hansen, L., Jickells, T.D., Knap, A.H., Reinhardt, K.H., Schneider, B., Soudine, A., Tokos, J.J., Tsunogai, S., Wollast, R., and Zhou, M., 1991. The atmospheric input of trace species to the world ocean. *Global Biogeochem. Cycles,* 5:193–259.

Dymond, J., Suess, E., and Lyle, M., 1992. Barium in deep-sea sediment: a geochemical proxy for paleoproductivity. *Paleoceanography,* 7:163–181.

Emerson, S.R., and Huested, S.S., 1991. Ocean anoxia and the concentrations of molybdenum and vanadium in seawater. *Mar. Chem.,* 34:177–196.

Francois, R., Honjo, S., Manganini, S.J., and Ravizza, G.E., 1995. Biogenic barium fluxes to the deep sea: implications for paleoproductivity reconstruction. *Global Biogeochem. Cycles,* 9:289–303.

Franklin, M.L., and Morse, J.W., 1983. The interaction of manganese(II) with the surface of calcite in dilute solutions and seawater. *Mar. Chem.,* 12:241–254.

Froelich, P.N., Arthur, M.A., Burnett, W.C., Deakin, M., Hensley, V., Jahnke, R., Kaul, L., Kim, K.H., Roe, K., Soutar, A., and Vathakanon, C., 1988. Early diagenesis of organic matter in Peru margin sediments: phosphorite precipitation. *Mar. Geol.,* 80:309–343.

Gingele, F., and Dahmke, A., 1994. Discrete barite particle and barium as tracers of paleoproductivity in South Atlantic sediments. *Paleoceanography,* 9:151–168.

Guo, Y., 1994. Primary productivity and phytoplankton in China Seas. *In* Zhou, Di, et al. (Eds.), *Oceanology of China Seas* (Vol. 1): Dordrecht (Kluwer Academic Publishers), 227–242.

Huang, Q., Wang W.-Z., Li, Y.S., and Li, C.W., 1994. Current characteristics of the South China Sea. *In* Zhou, Di, et al. (Eds.), *Oceanology of China Seas* (Vol. 1): Dordrecht (Kluwer Academic Publishers), 39–47.

Huerta-Diaz, M.A., and Morse, J.W., 1992. Pyritization of trace metals in anoxic marine sediments. *Geochim. Cosmochim. Acta,* 56:2681–2702.

Jacobs, L., and Emerson, S., 1985. Partitioning and transport of metals across the O_2-H_2S interface in a permanently anoxic basin: Framvaren Fjord, Norway. *Geochim. Cosmochim. Acta,* 49:1433–1444.

Martin, J.M., and Meybeck, M., 1979. Elemental mass-balance of material carried by major world rivers. *Mar. Chem.,* 7:173–206.

Mason, B., and Moore, C.B., 1985. *Grundzüge der Geochemie:* Stuttgart (Enke-Verlag).

McManus, J., Berelson, W.M., Klinkhammer, G.P., Johnson, K.S., Coale, K.H., Anderson, R.F., Kumar, N., Burdige, D.J., Hammond, D.E., Brumsack, H.-J., McCorkle,

D.C., and Rushdi, A., 1998. Geochemistry of barium in marine sediments: implications for its use as a paleoproxy. *Geochim. Cosmochim. Acta,* 62:3453–3473.

Milliman, J.D., and Meade, R.H., 1983. World wide delivery of river sediment to the oceans. *J. Geol.,* 91:1–21.

Molengraaff, G.A.F., 1921. Modern deep-sea research in the East Indian archipelago. *Geogr. J.,* 57:95–121.

Nesbitt, H.W., and Young, G.M., 1982. Early proterozoic climates and plate motions inferred from major element chemistry of lutites. *Nature,* 299:715–717.

Prakash Babu, C., Brumsack, H.-J., and Schnetger, B., 1999. Distribution of organic carbon in surface sediments along the eastern Arabian Sea: a revisit. *Mar. Geol.,* 162:91–104.

Rea, D.K., 1994. The paleoclimatic record provided by eolian deposition in the deep sea: the geologic history of wind. *Rev. Geophys.,* 32:159–195.

Ruttenberg, K.C., and Berner, R.A., 1993. Authigenic apatite formation and burial in sediments from non-upwelling, continental margin environments. *Geochim. Cosmochim. Acta,* 57:991–1007.

Schenau, S.J., Prins, M.A., De Lange, G.J., Monnin, C., 2001. Barium accumulation in the Arabian Sea: controls on barite preservation in marine sediments. *Geochim. Cosmochim. Acta*, 65:1545–1556.

Schneider, R.R., Price, B., Müller, P.J., Kroon, D., and Alexander, I., 1997. Monsoon-related variations in Zaire (Congo) sediment load and influence of fluvial silicate supply on marine productivity in the east equatorial Atlantic during the last 200,000 years. *Paleoceanography,* 12:463–481.

Schnetger, B., 1992. Chemical composition of loess from a local and worldwide view. *Neues. Jahrb. Mineral. Monatsh.,* 1992:29–47.

Shackleton, N.J., Crowhurst, S., Hagelberg, T., Pisias, N.G., and Schneider, D.A., 1995a. A new late Neogene time scale: application to Leg 138 sites. *In* Pisias, N.G., Mayer, L.A., Janecek, T.R., Palmer-Julson, A., and van Andel, T.H. (Eds.), *Proc. ODP, Sci. Results,* 138: College Station, TX (Ocean Drilling Program), 73–101.

Shackleton, N.J., Hall, M.A., and Pate, D., 1995b. Pliocene stable isotope stratigraphy of Site 846. *In* Pisias, N.G., Mayer, L.A., Janecek, T.R., Palmer-Julson, A., and van Andel, T.H. (Eds.), *Proc. ODP, Sci. Results,* 138: College Station, TX (Ocean Drilling Program), 337–355.

Shimmield, G.B., and Mowbray, S.R., 1991. The inorganic geochemical record of the northwest Arabian Sea: a history of productivity variation over the last 400 k.y. from Sites 722 and 724. *In* Prell, W.L., Niitsuma, N., et al., *Proc. ODP, Sci. Results,* 117: College Station, TX (Ocean Drilling Program), 409–429.

Shipboard Scientific Party, 2000. Site 1143. *In* Wang, P., Prell, W.L., Blum, P., et al., *Proc. ODP, Init. Repts.,* 184, 1–103 [CD-ROM]. Available from: Ocean Drilling Program, Texas A&M University, College Station TX 77845-9547, USA.

Szalay, A., and Szilagyi, M., 1967. The association of vanadium with humic acids. *Geochim. Cosmochim. Acta,* 31:1–6.

Taylor, S.R., and McLennan, S.M., 1985. *The Continental Crust: Its Composition and Evolution:* Oxford (Blackwell Scientific).

Thomson, J., Higgs, N.C., Jarvis, I., Hydes, D.J., Colley, S., and Wilson, T.R.S., 1986. The behaviour of manganese in Atlantic carbonate sediments. *Geochim. Cosmochim. Acta,* 50:1807–1818.

Thunell, R.C., Qingmin, M., Calvert, S.E., and Pedersen, T.F., 1992. Glacial-Holocene biogenic sedimentation patterns in the South China Sea: productivity variations and surface water pCO_2. *Paleoceanography,* 7:143–162.

Thurow, J., Brumsack, H.-J., Rullkötter, J., Littke, R., and Meyers, P., 1992. The Cenomanian/Turonian boundary event in the Indian Ocean—a key to understanding the global picture. *In* Duncan, R.A., Rea, D.K., Kidd, R.B., von Rad, U., and Weissel, J.K. (Eds.), *Synthesis of Results from Scientific Drilling in the Indian Ocean.* Geophys. Monogr., Am. Geophys. Union, 70:253–273.

Tiedemann, R., and Franz, S.O., 1997. Deep-water circulation, chemistry, and terrigenous sediment supply in the equatorial Atlantic during the Pliocene, 3.3–2.6 Ma and 5–4.5 Ma. *In* Shackleton, N.J., Curry, W.B., Richter, C., and Bralower, T.J. (Eds.), *Proc. ODP, Sci. Results,* 154: College Station, TX (Ocean Drilling Program), 299–318.

Tiedemann, R., Sarnthein, M., and Shackleton, N.J., 1994. Astronomic timescale for the Pliocene Atlantic $\delta^{18}O$ and dust flux records of Ocean Drilling Program Site 659. *Paleoceanography,* 9:619–638.

Van Cappellen, P., and Berner, R.A., 1988. A mathematical model for the early diagenesis of phosphorus and flourine in marine sediments: apatite precipitation. *Amer. J. Sci.,* 288:289–333.

Van Cappellen, P., and Ingall, E.D., 1994. Benthic phosphorus regeneration, net primary production, and ocean anoxia: a model of the coupled marine biogeochemical cycles of carbon and phosphorus. *Paleoceanography,* 9:677–692.

Venkatarathnam, K., and Ryan, W.B.F., 1971. Dispersal patterns of clay minerals in the sediments of the eastern Mediterranean Sea. *Mar. Geol.,* 11:261–282.

Wang, L., and Wang, P., 1990. Late Quaternary paleoceanography of the South China Sea: glacial interglacial contrasts in an enclosed basin. *Paleoceanography,* 5:77–90.

Wang, P., Prell, W.L., Blum, P., et al., 2000. *Proc. ODP, Init. Repts.,* 184 [CD-ROM]. Available from: Ocean Drilling Program, Texas A&M University, College Station, TX 77845-9547, USA.

Wang, P., Wang, L., Yunhua, B., and Zhimin, J., 1995. Late Quaternary paleoceanography of the South China Sea: surface circulation and carbonate cycles. *Mar. Geol.,* 127:145–165.

Wedepohl, K.H., 1971. Environmental influences on the chemical composition of shales and clays. *In* Ahrens, L.H., Press, F., Runcorn, S.K., and Urey, H.C. (Eds.), *Physics and Chemistry of the Earth:* Oxford (Pergamon), 307–331.

————, 1991. The composition of the upper Earth's crust and the natural cycles of selected metals: metals in natural raw materials; natural resources. *In* Merian, E. (Ed.), *Metals and Their Compounds in the Natural Environment:* Weinheim (VCH-Verlagsges.), 3–17.

Wehausen, R., 1999. Anorganische Geochemie zyklischer Sedimente aus dem östlichen Mittelmeer: rekonstruktion der Paläoumweltbedingungen [Thesis Dr. Rer. Nat.]. Oldenburg, Carl von Ossietzky University.

Wehausen, R., and Brumsack, H.-J., 1999. Cyclic variations in the chemical composition of eastern Mediterranean Pliocene sediments: a key for understanding sapropel formation. *Mar. Geol.,* 153:161–176.

————, 2000. Chemical cycles in Pliocene sapropel bearing and sapropel barren eastern Mediterranean sediments. *Palaeogeogr., Palaeoclimatol., Palaeoecol.,* 158:325-352.

————, 2002. Astronomical forcing of the East Asian monsoon mirrored by the composition of Pliocene South China Sea sediments. *Earth Planet. Sci. Lett.,* 201:621–636.

Figure F1. Map showing ODP Leg 184 Sites in the South China Sea. The investigated ODP Site 1143 in the southern South China Sea is shown in bold.

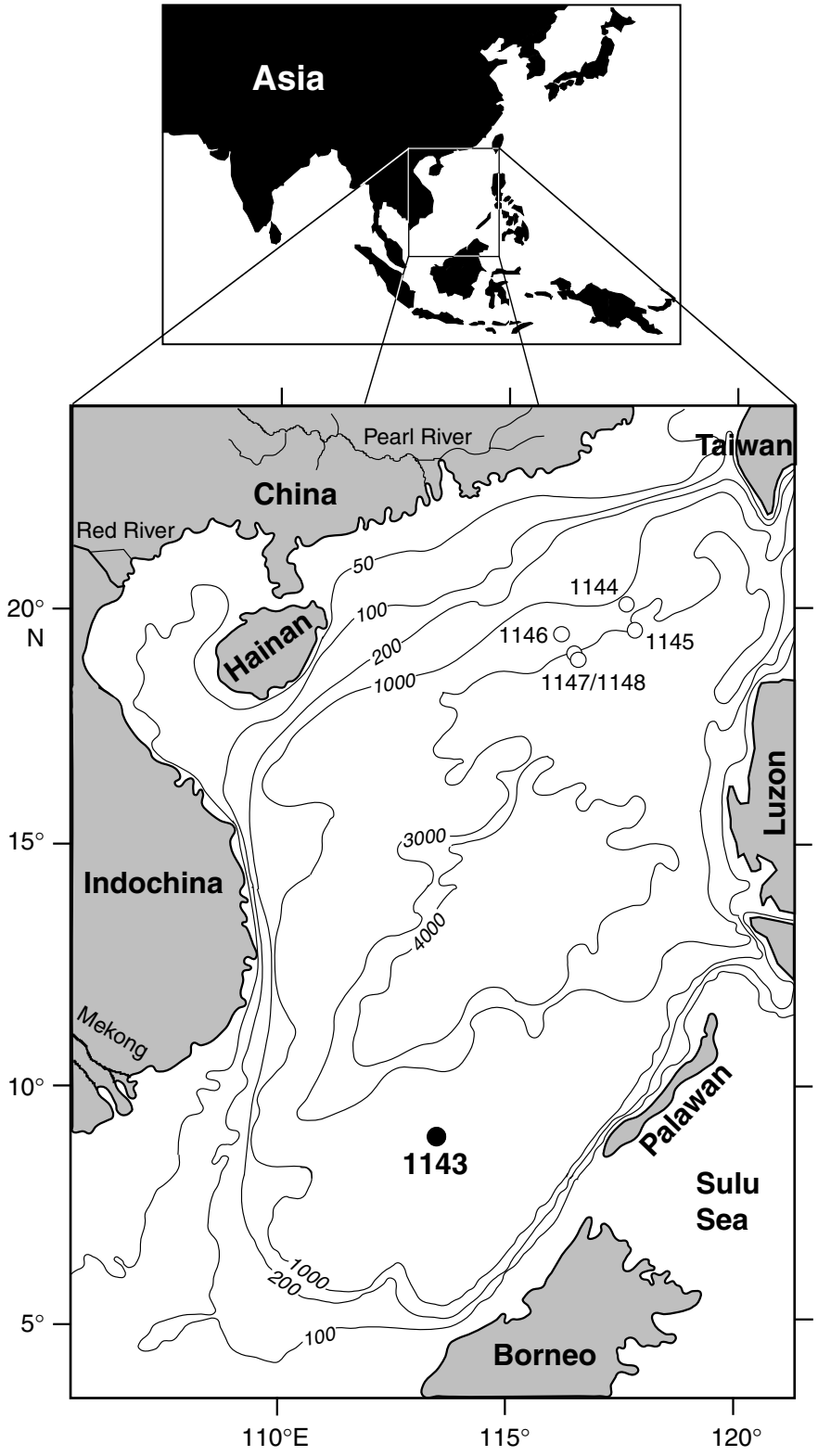

Figure F2. Correlation of CaO (measured by XRF) and carbonate carbon (C_{carb}) values (measured by coulometry).

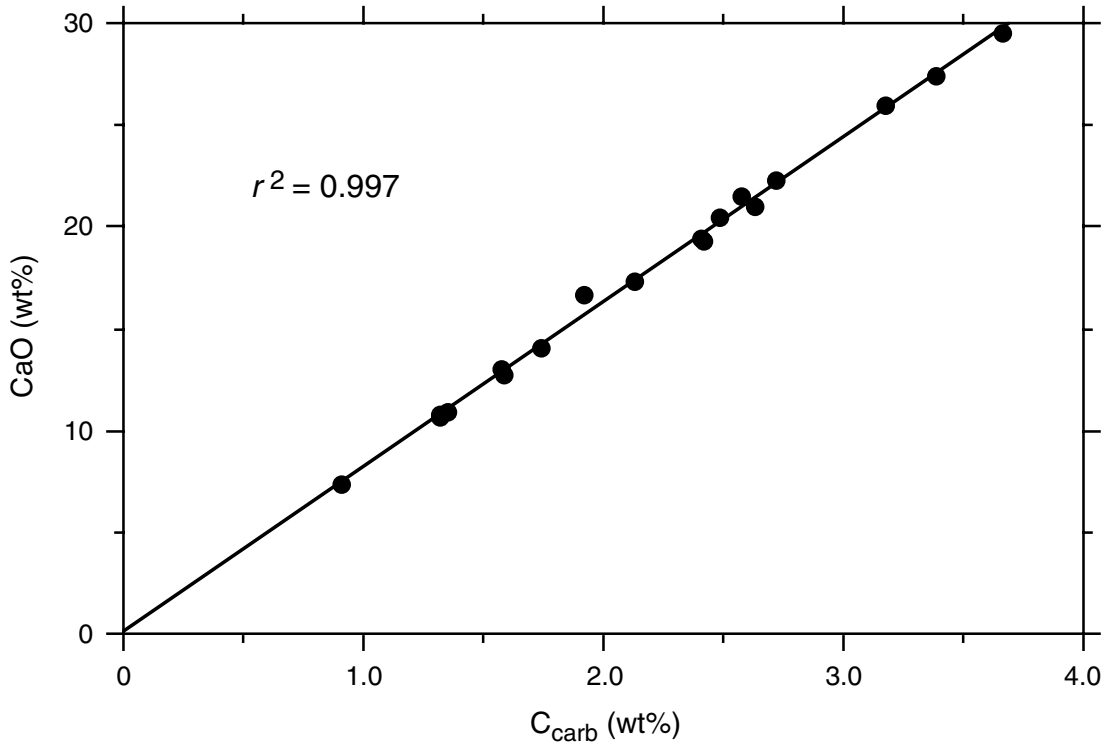

Figure F3. Ternary plot of SiO_2 (representing quartz or biogenic silica), Al_2O_3 (representing clay minerals), and CaO (representing carbonate) contents. Average shale data point from Wedepohl (1971).

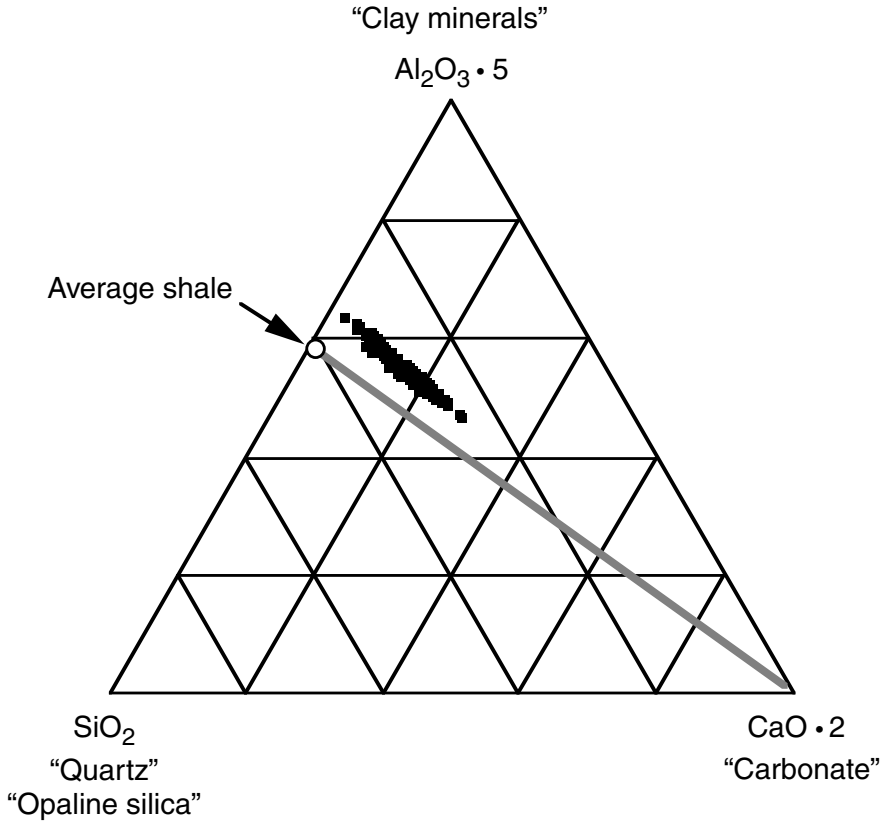

Figure F4. Correlation of TiO_2 and Al_2O_3 contents. Data for Site 1145 samples are taken from Wehausen and Brumsack (2002), average loess data are taken from Schnetger (1992), and Mekong riverine SPM data are from Martin and Meybeck (1979).

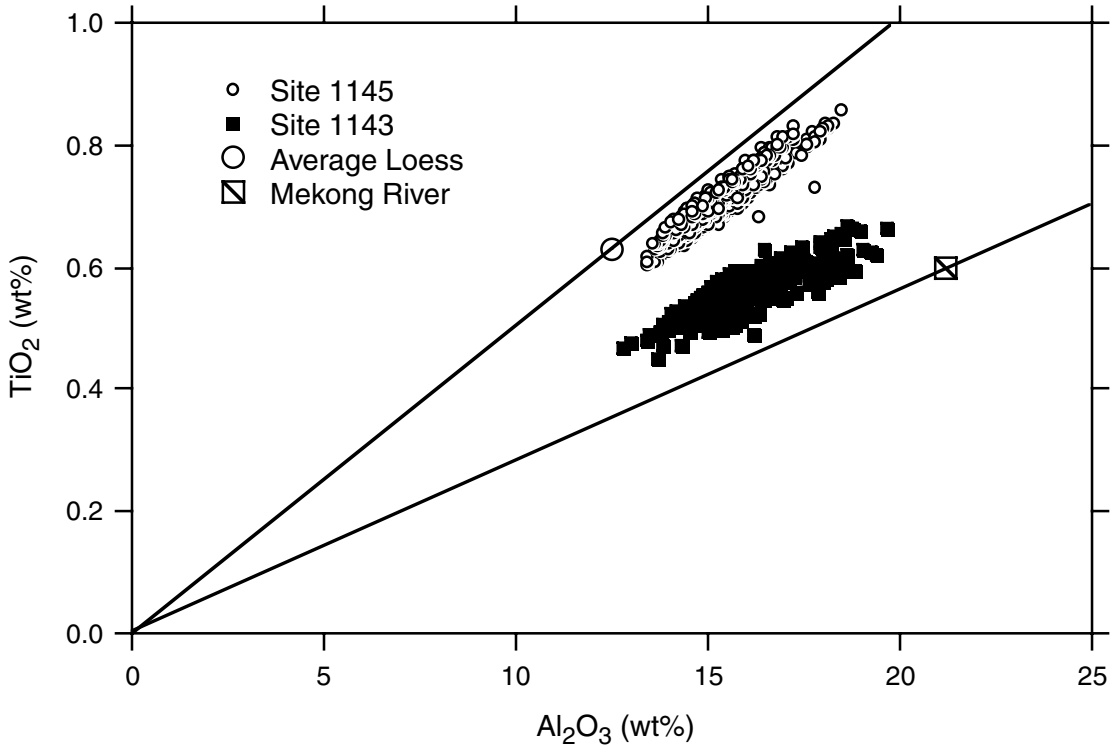

Figure F5. Benthic foraminifer $\delta^{18}O$ records (**Cheng et al.,** this volume) and bulk geochemical data for $CaCO_3$, SiO_2, and Al_2O_3. Stratigraphy and oxygen isotope stages (OIS) from **Tian et al.** (this volume). Bold lines in the geochemical records indicate the 50-point running average. *C. wullerst.* = *Cibicidoides wuellerstorfi*.

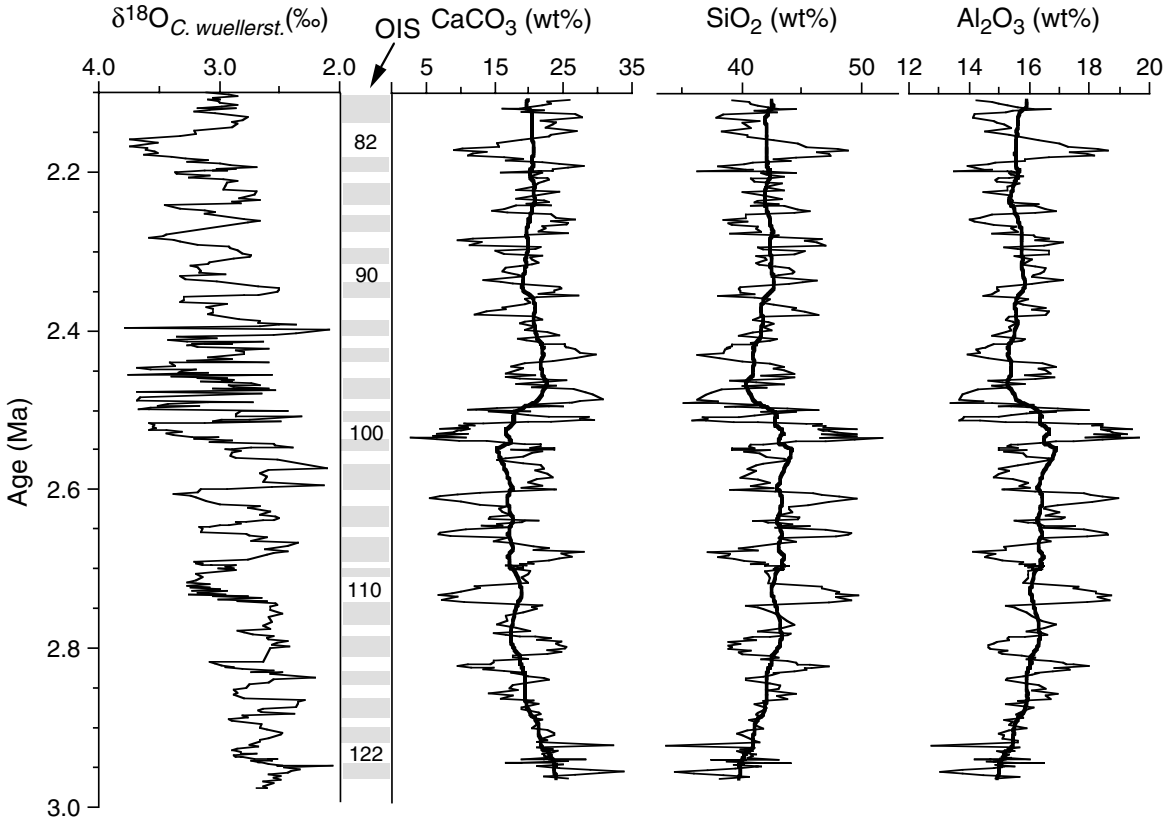

Figure F6. Records of terrigenous detrital element contents and elemental ratios. **A.** Comparison of SiO_2 (cfb) and Al_2O_3 (cfb) contents with Si/Al ratio, TiO_2 (cfb) content, and K_2O (cfb) content. (Continued on next page).

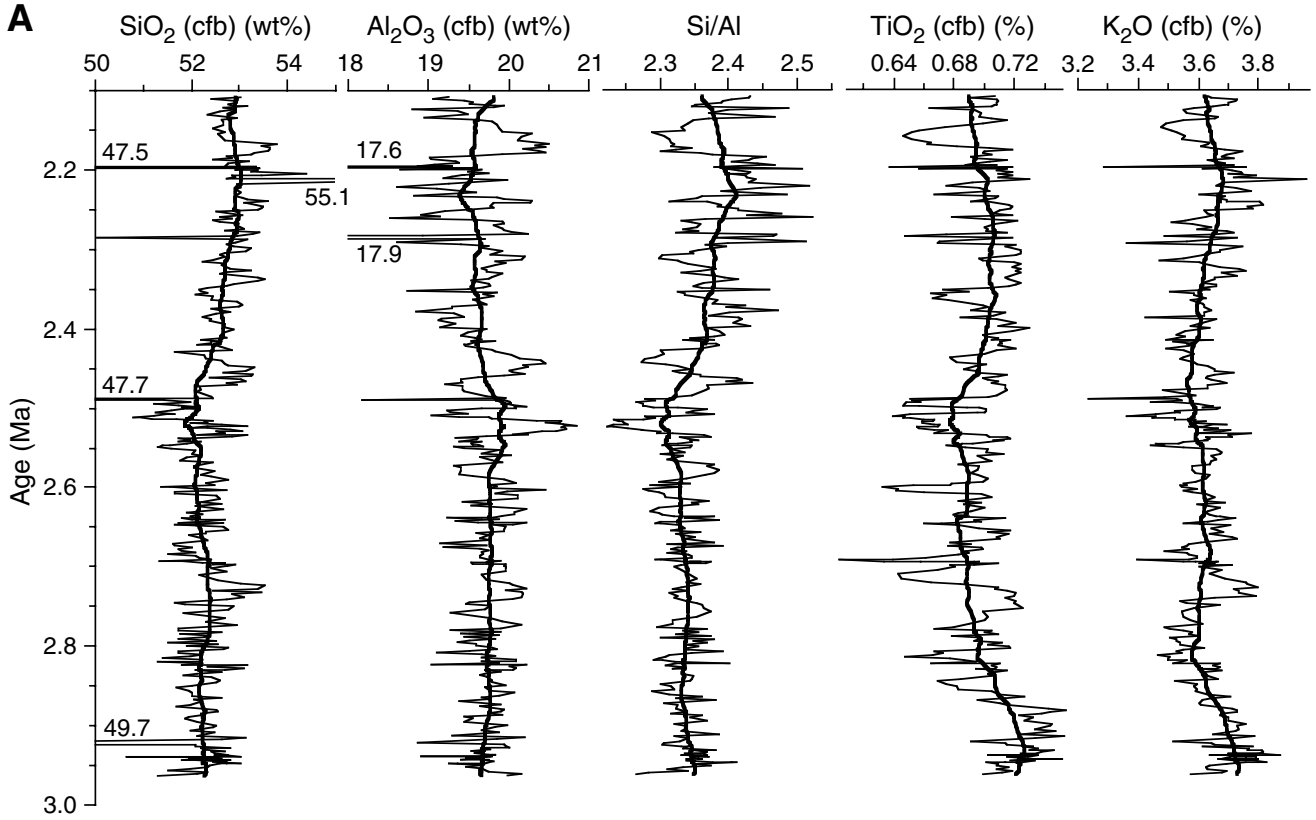

Figure F6 (continued). **B**. Comparison of major element records (Ti/Al and K/Al ratios) with trace element aluminium ratios (Cr/Al, Rb/Al, and Zr/Al). The index cfb indicates that the contents were calculated on a carbonate-free basis (see "Material and Methods" p. 2). Bold lines indicate the 50-point running average value.

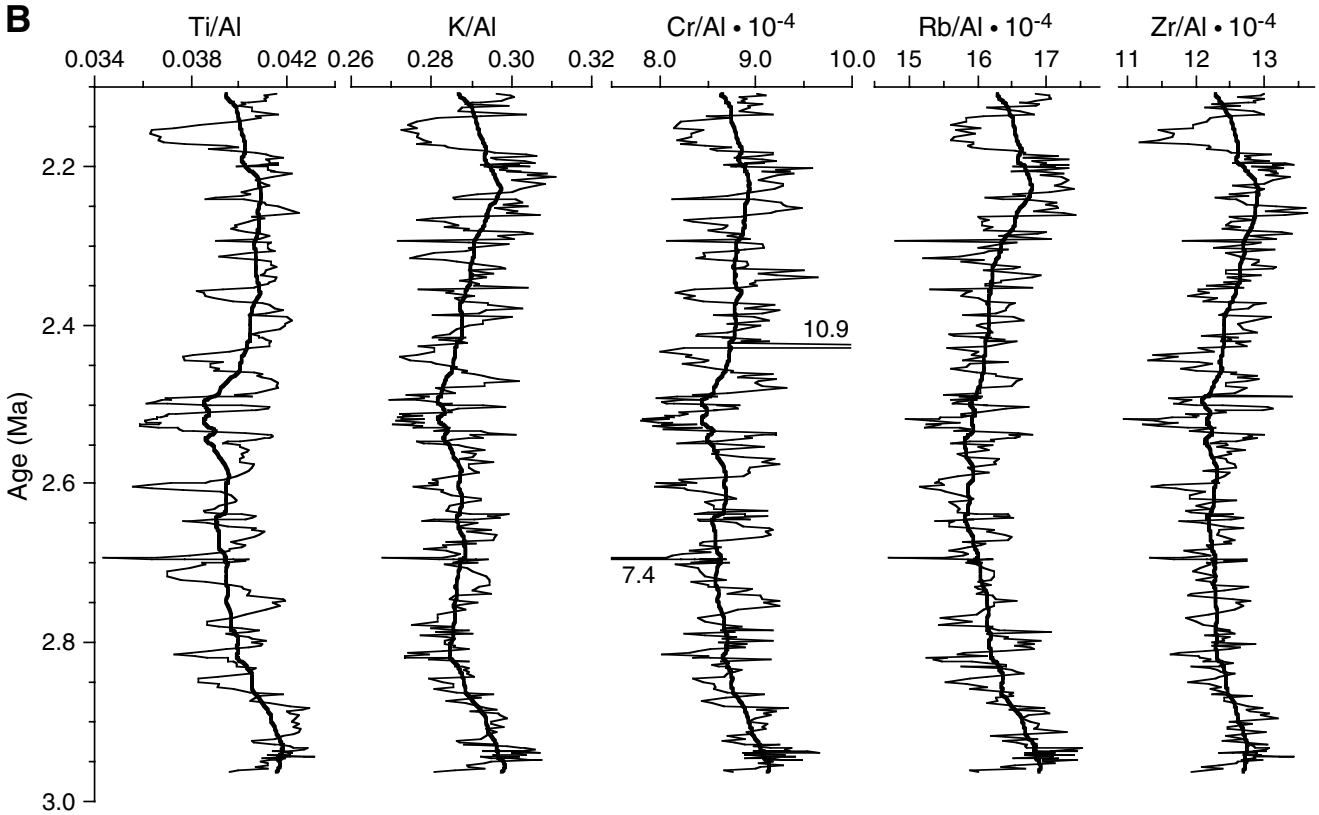

Figure F7. Comparison of the benthic foraminifer $\delta^{18}O$ record (**Cheng et al.**, this volume) and terrigenous detrital element parameters. Al_2O_3 (cfb) and TiO_2 (cfb) contents calculated on a carbonate-free basis (see **"Material and Methods,"** p. 2). Bold lines in the geochemical records indicate the 50-point running average. Stratigraphy and oxygen isotope stages (OIS) from **Tian et al.** (this volume). Horizontal shaded bands indicate interglacial periods.

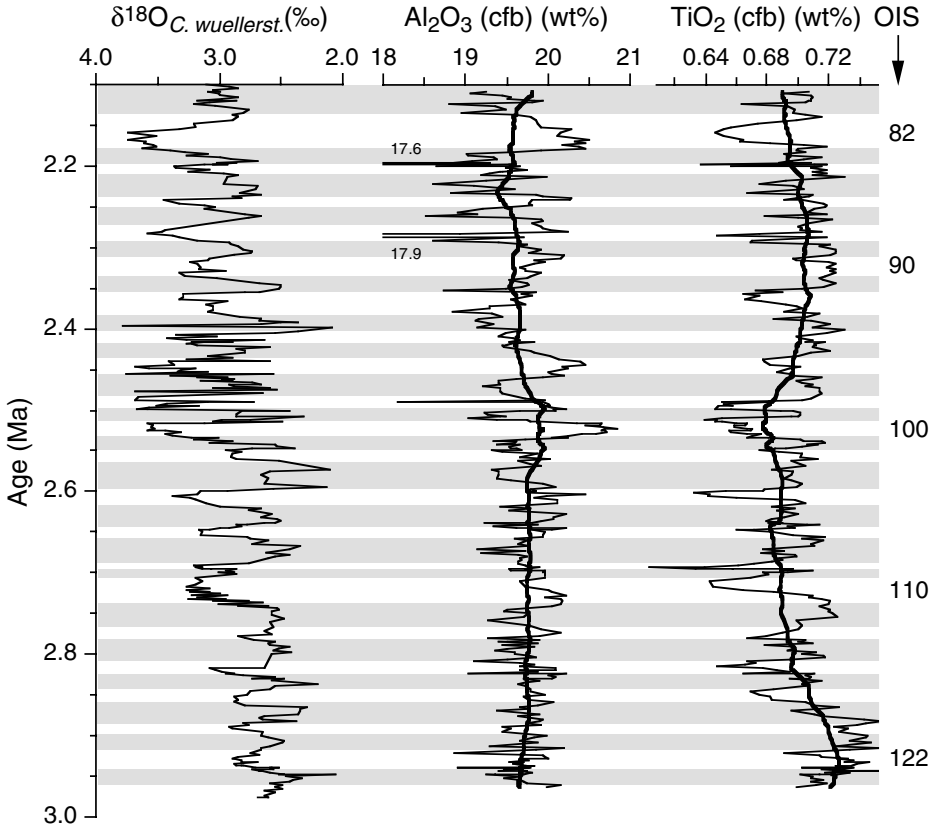

Figure F8. Comparison of the benthic foraminifer $\delta^{18}O$ record (**Cheng et al.,** this volume) and the records of biologically influenced element parameters: Ba/Al ratio, P/Al ratio, and $CaCO_3$ content. Stratigraphy and oxygen isotope stages (OIS) from **Tian et al.** (this volume). Shaded areas indicate interglacial periods. Average shale data are from Wedepohl (1971, 1991). *C. wuellerst.* = *Cibicidoides wuellerstorfi*.

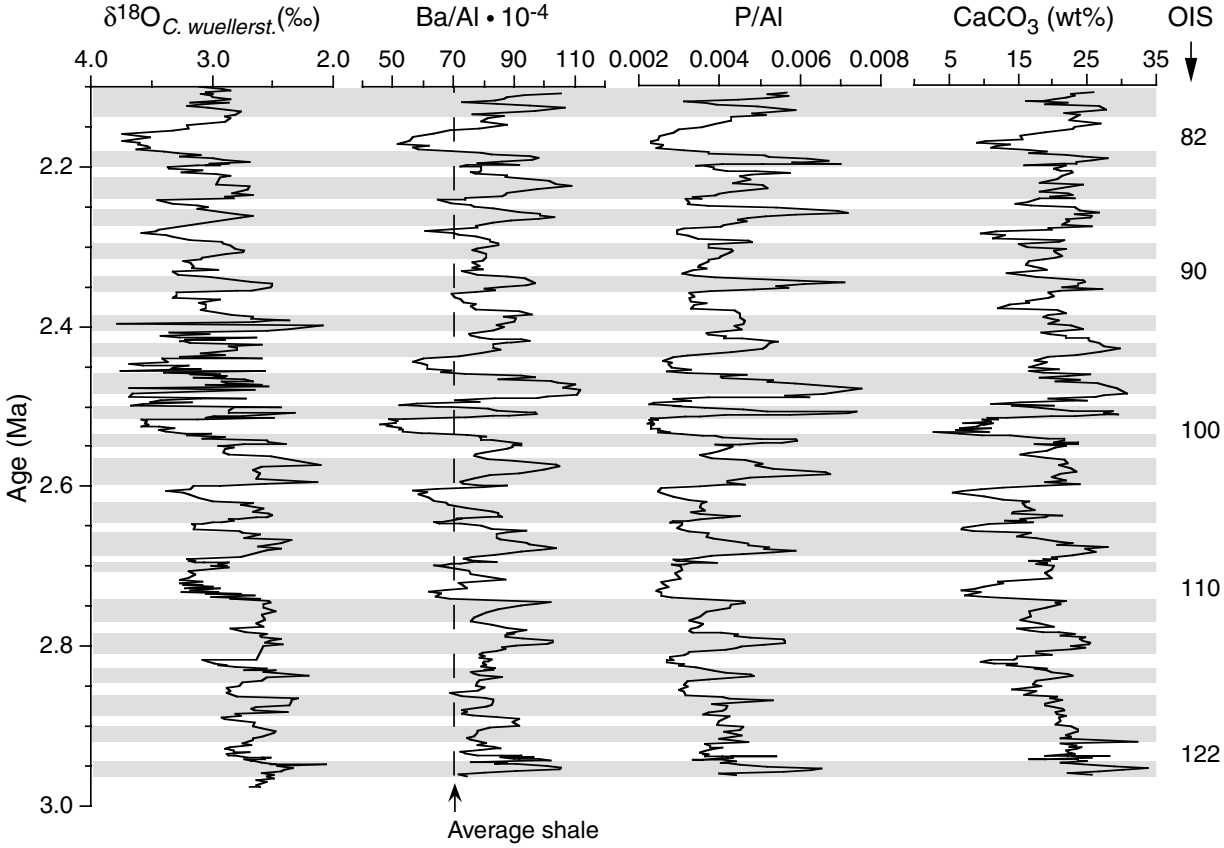

Figure F9. Profiles of elements that may be overprinted by diagenesis or redox reactions in the water column. **A.** Records of Fe_2O_3 calculated on a carbonate-free basis (cfb), As/Al ratio, and Mn/Al ratio compared to $CaCO_3$ content. **B.** Records of Co/Al, Ni/Al, and V/Al ratios. Data for the upper continental crust are from Taylor and McLennan (1985), average loess from Schnetger (1992), average shale from Wedepohl (1971, 1991), and Mekong suspended matter (SPM) from Martin and Meybeck (1979).

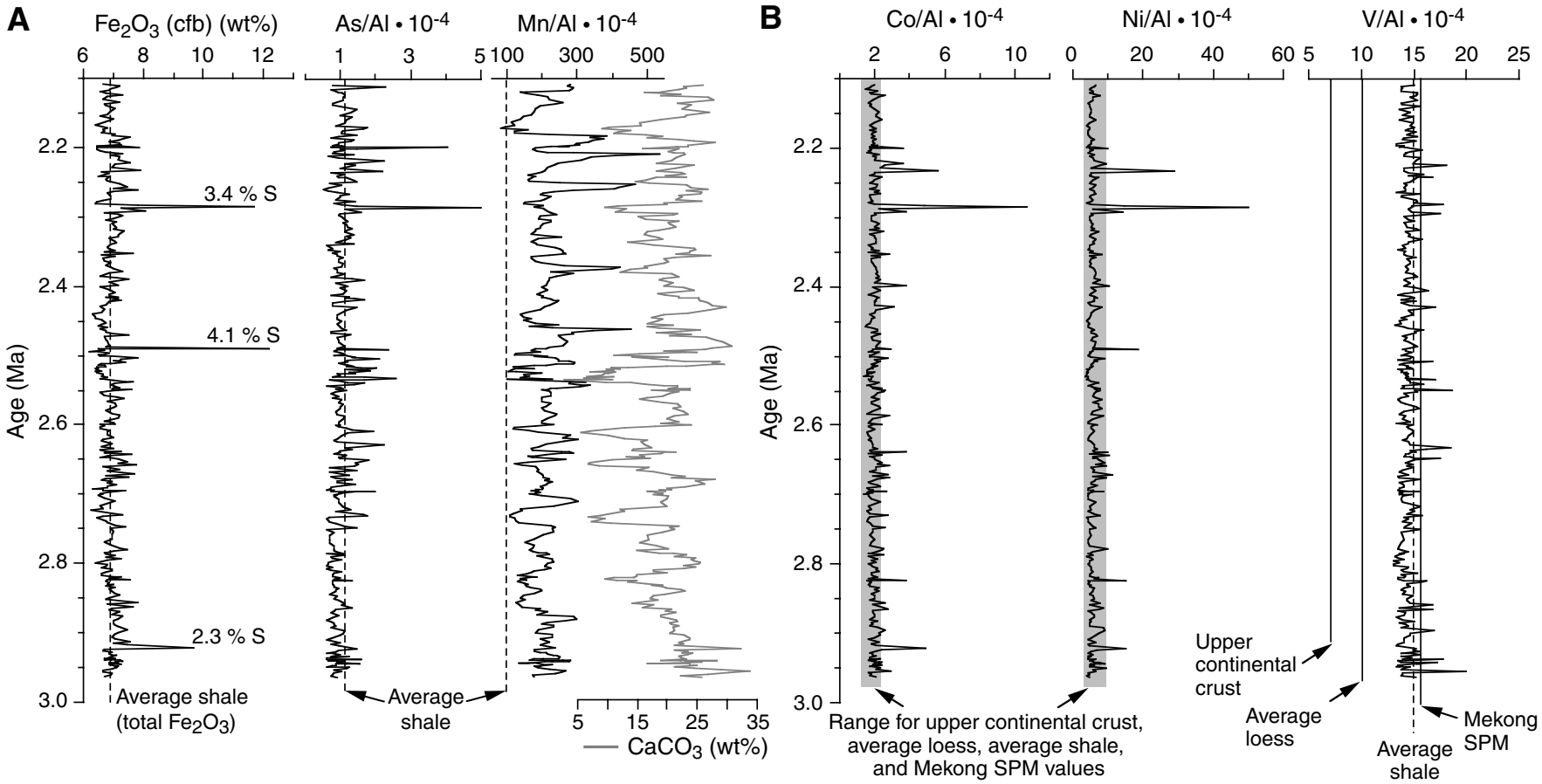

Table T1. Inorganic geochemical data for late Pliocene sediments, Site 1143.

Core, section, interval (cm)	Depth (mcd)	SiO_2 (wt%)	TiO_2 (wt%)	Al_2O_3 (wt%)	Fe_2O_3 (wt%)	MnO (wt%)	CaO (wt%)	K_2O (wt%)	P_2O_5 (wt%)	As (µg/g)	Ba (µg/g)	Co (µg/g)	Cr (µg/g)	Ni (µg/g)	Rb (µg/g)	Sr (µg/g)	V (µg/g)	Zr (µg/g)	C_{carb} (wt%)	C_{org} (wt%)
184-1143B-																				
11H-2, 0–1	99.50	39.2	0.523	14.3	4.94	0.275	14.56	2.69	0.098	6	798	15	68	49	127	608	114	98		
11H-2, 10–11	99.60	40.6	0.535	14.8	5.60	0.273	12.64	2.82	0.093	18	732	14	71	46	133	530	107	101		
11H-2, 20–21	99.70	40.8	0.545	15.0	5.47	0.294	12.91	2.87	0.104	12	697	14	70	40	135	526	110	100		
11H-2, 30–31	99.80	41.4	0.554	15.3	5.41	0.299	12.25	2.91	0.096	6	701	12	72	38	138	509	112	105		
11H-2, 40–41	99.90	42.2	0.566	15.6	5.49	0.293	11.22	2.96	0.084	7	693	18	73	46	139	477	114	106		
11H-2, 50–51	100.00	43.0	0.576	16.2	5.35	0.173	10.43	3.01	0.063	8	629	16	76	47	143	464	131	110		
11H-2, 60–61	100.10	44.6	0.592	16.7	5.55	0.159	9.08	3.09	0.063	9	642	15	78	41	147	425	135	113		
11H-2, 70–71	100.20	41.0	0.549	15.4	5.26	0.164	12.41	2.84	0.069	9	688	15	74	50	138	576	126	100		
11H-2, 80–81	100.30	42.9	0.538	15.3	5.92	0.194	10.57	2.91	0.073	9	771	21	72	64	136	476	123	102		
11H-2, 90–91	100.40	38.5	0.507	14.2	4.97	0.209	15.02	2.60	0.085	8	799	17	67	43	121	638	110	91		
11H-2, 100–101	100.50	37.9	0.505	14.1	4.82	0.214	15.48	2.58	0.101	8	726	14	66	42	124	657	115	96		
11H-2, 110–111	100.60	41.4	0.545	14.8	5.64	0.264	12.20	2.87	0.086	6	600	13	72	33	132	496	108	102		
11H-2, 120–121	100.70	40.0	0.536	14.9	5.10	0.243	13.39	2.78	0.093	6	683	14	67	38	127	548	110	98		
11H-2, 130–131	100.80	40.3	0.548	15.2	5.17	0.200	13.11	2.72	0.079	8	655	14	70	39	127	541	125	98		
11H-2, 140–141	100.90	40.8	0.542	15.4	5.47	0.189	12.60	2.71	0.080	12	646	16	67	41	129	523	111	99		
11H-3, 0–1	101.00	38.3	0.493	14.5	5.04	0.175	15.06	2.54	0.069	10	673	17	63	40	120	621	113	92		
11H-3, 10–11	101.10	40.5	0.505	15.3	5.22	0.177	12.95	2.70	0.066	8	635	17	66	38	130	548	113	97		
11H-3, 20–21	101.20	40.5	0.503	15.7	5.07	0.158	12.82	2.72	0.057	11	568	17	70	39	130	533	124	95		
11H-3, 30–31	101.30	42.6	0.523	16.3	5.66	0.156	10.65	2.88	0.057	10	550	21	72	55	138	464	118	101		
11H-3, 40–41	101.40	44.6	0.552	17.0	5.69	0.132	8.62	3.00	0.052	10	510	18	75	42	141	405	134	105		
11H-3, 50–51	101.50	45.4	0.561	17.3	5.39	0.141	8.72	3.07	0.052	8	507	16	75	34	143	399	134	105		
11H-3, 60–61	101.60	48.0	0.595	18.3	5.93	0.116	5.72	3.26	0.051	17	519	18	81	44	154	305	145	108		
11H-3, 70–71	101.70	48.8	0.620	18.6	6.18	0.105	5.09	3.28	0.052	16	505	20	81	48	157	282	143	117		
11H-3, 80–81	101.80	46.2	0.606	17.4	5.74	0.192	7.77	3.14	0.055	10	568	16	78	38	146	356	131	112		
11H-3, 90–91	101.90	47.2	0.633	17.9	5.91	0.147	6.70	3.25	0.056	10	541	20	83	43	151	327	144	116		
11H-3, 100–101	102.00	47.4	0.622	18.2	5.85	0.148	6.27	3.33	0.054	10	564	18	82	40	155	308	141	117		
11H-3, 110–111	102.10	44.6	0.585	16.7	5.91	0.252	9.10	3.12	0.063	13	611	16	76	40	146	399	127	110		
11H-3, 120–121	102.20	42.7	0.570	15.9	5.63	0.417	10.68	2.99	0.072	8	665	17	77	40	140	446	129	105		
11H-3, 130–131	102.30	44.1	0.576	15.9	6.30	0.366	9.29	3.07	0.072	6	694	15	77	45	140	403	118	110		
11H-3, 140–141	102.40	40.9	0.542	14.9	5.75	0.380	12.32	2.90	0.092	11	747	16	71	46	135	503	109	100		
11H-4, 0–1	102.50	40.3	0.541	14.6	5.41	0.345	13.63	2.75	0.093	10	762	15	68	40	129	554	118	99		
11H-4, 10–11	102.60	38.0	0.507	14.0	4.95	0.317	15.64	2.64	0.105	7	710	14	67	38	128	626	106	94		
11H-4, 20–21	102.70	39.2	0.516	14.2	5.36	0.290	14.40	2.74	0.115	7	647	15	69	38	126	569	100	98		
11H-4, 30–31	102.80	40.4	0.527	14.5	5.54	0.289	13.05	2.82	0.107	6	598	14	68	32	130	521	102	96		
11H-4, 40–41	102.90	40.9	0.543	14.8	5.55	0.310	13.09	2.85	0.104	8	634	17	71	38	133	530	110	104		
11H-4, 50–51	103.00	36.4	0.488	13.5	4.94	0.229	13.08	2.52	0.115	8	656	15	62	34	121	541	98	96		
11H-4, 60–61	103.10	41.8	0.562	15.3	5.36	0.287	12.19	2.94	0.094	6	603	14	72	32	140	505	114	106		
11H-4, 70–71	103.20	41.8	0.558	15.4	5.72	0.238	12.03	2.92	0.076	33	608	20	71	48	138	489	115	108		
11H-4, 80–81	103.30	44.5	0.552	15.7	6.60	0.195	8.93	3.04	0.065	12	599	30	73	81	142	404	124	109		
11H-4, 90–91	103.40	41.6	0.558	15.3	5.05	0.192	12.33	2.87	0.068	8	641	14	71	38	134	541	121	104		
184-1143C-																				
11H-4, 100–101	103.50	42.0	0.559	15.4	5.11	0.181	11.82	2.93	0.072	9	645	15	78	46	141	533	128	108		
11H-4, 110–111	103.60	43.5	0.574	15.8	5.24	0.199	11.24	2.99	0.074	7	662	14	77	40	142	492	123	108		
11H-4, 120–121	103.70	42.2	0.562	15.4	5.35	0.227	11.79	2.96	0.078	7	639	15	76	39	134	490	116	107		
11H-4, 130–131	103.80	40.8	0.548	15.0	5.24	0.295	12.75	2.86	0.089	6	602	12	72	35	134	511	114	104		
11H-4, 140–141	103.90	40.9	0.555	14.9	5.63	0.545	12.77	2.93	0.104	11	610	18	74	48	136	504	111	104		
11H-5, 0–1	104.00	41.1	0.553	15.0	5.40	0.421	12.35	2.90	0.087	6	696	15	73	37	134	486	111	103		

Note: Only a portion of this table appears here. The complete table is available in **ASCII**.